Supporting Information

Self-aligned plasmonic nanopore by optically controlled dielectric breakdown

Sergii Pud[†]*, Daniel Verschueren*[†]*, Nikola Vukovic, Calin Plesa, Magnus Jonsson*[**] *and Cees Dekker*[*]

Department of Bionanoscience, Kavli Institute of Nanoscience, Delft University of Technology, Lorentzweg 1, 2628 CJ Delft, The Netherlands

E-mail: c.dekker@tudelft.nl

[*] To whom correspondence should be addressed

[**]Current address: Organic Electronics, Department of Science and Technology, Campus Norrköping, Linköping University, SE-60174 Norrköping, Sweden

1. TEM images of plasmonic nanopores fabricated using plasmonic dielectric breakdown in longitudinal polarization
2. Nanopore fabricated using laser-promoted (non-plasmonic) dielectric breakdown
3. Nanopore fabricated using regular dielectric breakdown (no laser) in plasmonic membrane
4. FDTD simulations of field enhancements and absorption cross-sections of bowtie nanoantennas
5. Estimation of the optical field strength
6. Noise spectra of plasmonic-breakdown-fabricated nanopore
7. Conductance versus diameter of plasmonic-breakdown-fabricated nanopores
8. Diameter and conductance determination of plasmonic nanopore used in DNA translocations
9. Current increase versus laser power for the plasmonic nanopore used in DNA translocations

1. TEM images of plasmonic nanopores fabricated using plasmonic dielectric breakdown in longitudinal polarization

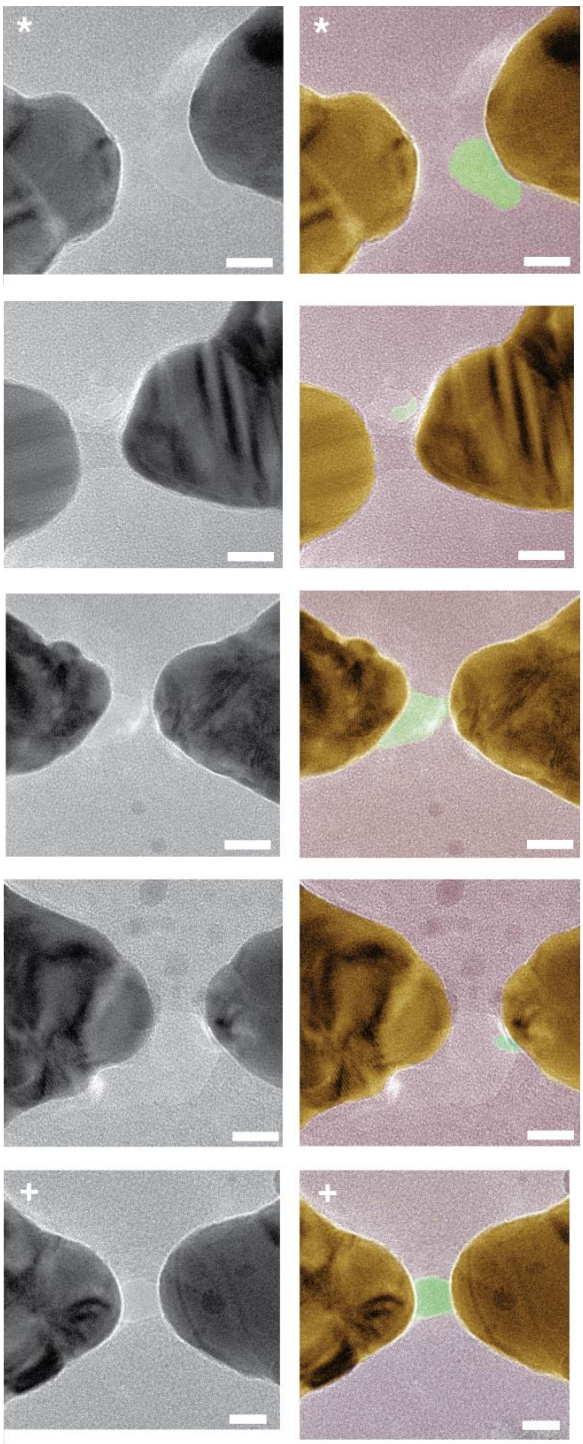

Figure S1. Examples of original and false colored TEM images of plasmonic nanopores drilled using plasmonic promoted dielectric breakdown in longitudinal mode. Scale bars are 10 nm. The TEM image of the nanopore used for the DNA translocations is indicated with a star: the image used in figure 4D in the main text is indicated with a plus sign.

2. Nanopore fabricated using laser-promoted (non-plasmonic) dielectric breakdown

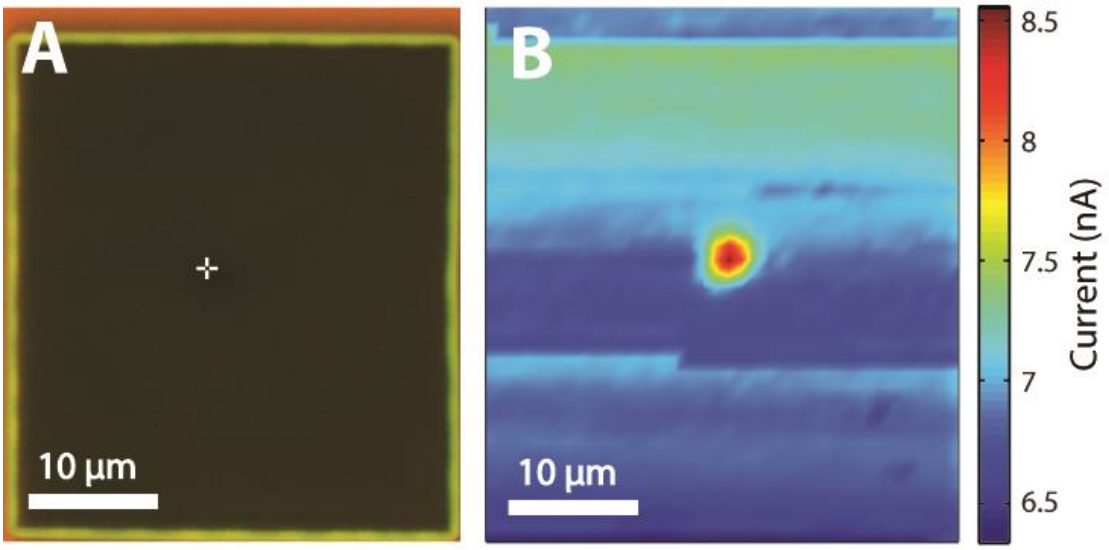

Figure S2. Laser-promoted dielectric-breakdown-fabricated nanopore. (A) Position of laser focus before dielectric breakdown. (B) Ionic-current map of the membrane, scanned at 100 mV bias and 45 mW of laser power in 1 µm size steps.

To show that the plasmonic dielectric breakdown is promoted by the optical field rather than heating from the plasmonic nanostructure, we fabricated a nanopore using dielectric breakdown promoted using the laser only (i.e. without the presence of any plasmonic structure). Figure S2.A shows the optical image of a membrane before dielectric breakdown, where the white cross is indicating the laser location. Directly after the formation of a nanopore, drilled at $V_m = 6$ V in 2 M LiCl and 45 mW, we scanned the membrane at 45 mW to visualize the location of the nanopore[1] (Figure S2.B). A clear current increase was observed at the location the laser was initially placed, indicating the laser illumination localized the dielectric breakdown to the desired position.

3. Nanopore fabricated using regular dielectric breakdown (no laser) in plasmonic membrane

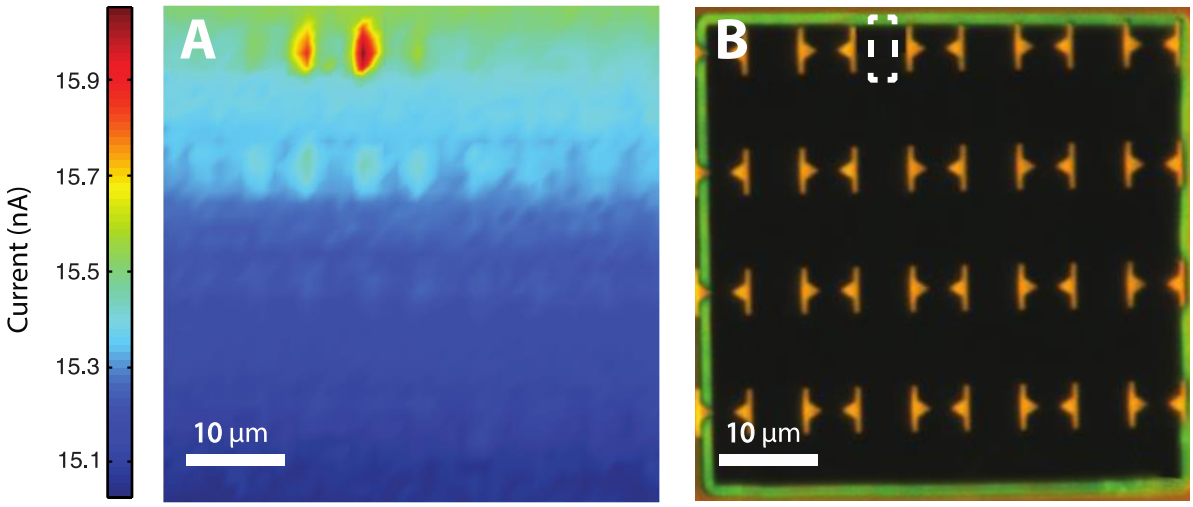

Figure S3. Regular dielectric breakdown in plasmonic membrane. (A) Ionic current map of the membrane, scanned in 1µm size steps at 50 mV bias and 1 mW of laser power in longitudinal mode. (B) Optical image of the membrane, where the region of expected pore location is indicated.

To show that the plasmonic dielectric breakdown localizes nanopore formation due to plasmon excitation, we fabricated a nanopore in a plasmonic membrane using regular dielectric breakdown, i.e. without any laser illumination. Figure S3.A shows the result of a membrane scan after nanopore formation, drilled at $V_m = 7$ V in 2 M LiCl. Two regions of small current enhancement are clearly distinguishable. In each of these regions a gold alignment-marker structure is located, which heats up its immediate surroundings when illuminated with the laser. This heating will cause a measurable current increase through the nanopore, if the pore has formed in the proximity of the marker structure. Since laser illumination of two markers leads to a current increase, we infer that the nanopore is located in between both alignment-markers. Figure S3.B shows an optical image of the membrane, where the region of expected pore location (in between 2 marker structures) is indicated. Note

that direct illumination of the nanopore at low laser power will cause an insufficient current increase to be observed, as no plasmonic structures are present on top of it.

4. FDTD simulations of field enhancements and absorption cross-sections of the bowtie

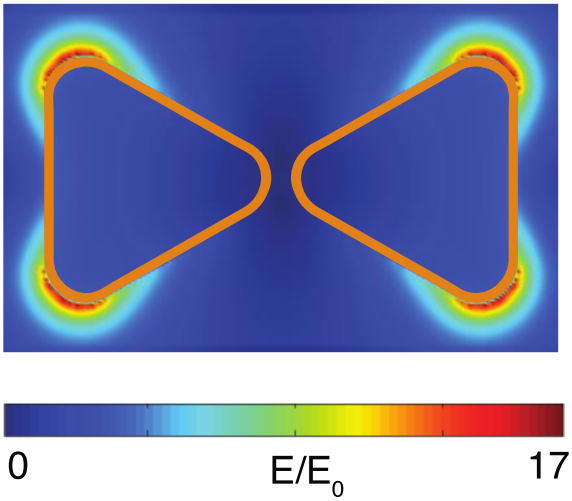

Figure S4. FDTD simulation of the electric field E/E_0 at 785 nm wavelength for the bowtie antenna as described in the main text, illuminated in transverse polarization. The bowtie is outlined by the orange frame.

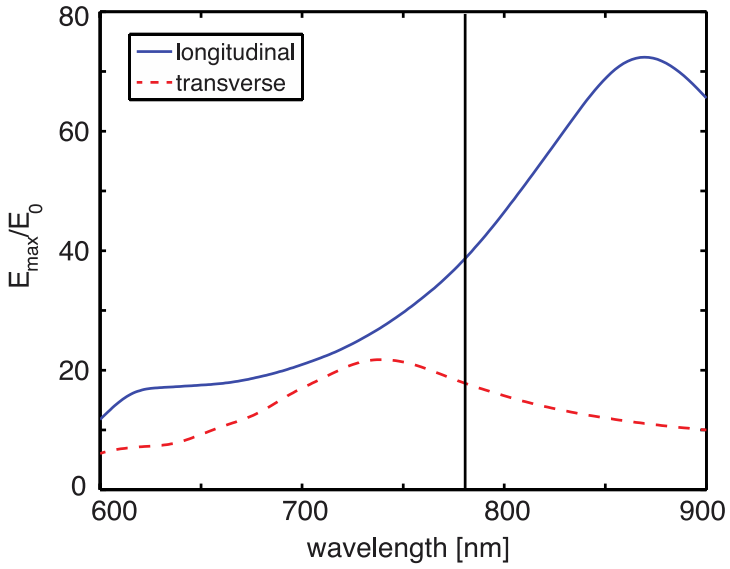

Figure S5. FDTD simulation of the maximum electric field enhancement E_{max}/E_0 as a function of wavelength for bowtie nanoantennas as described in the main text. The blue full line and the red dashed line show the results for longitudinal and transverse excitation. The excitation wavelength (785 nm) as used in our setup is indicated with a vertical black line.

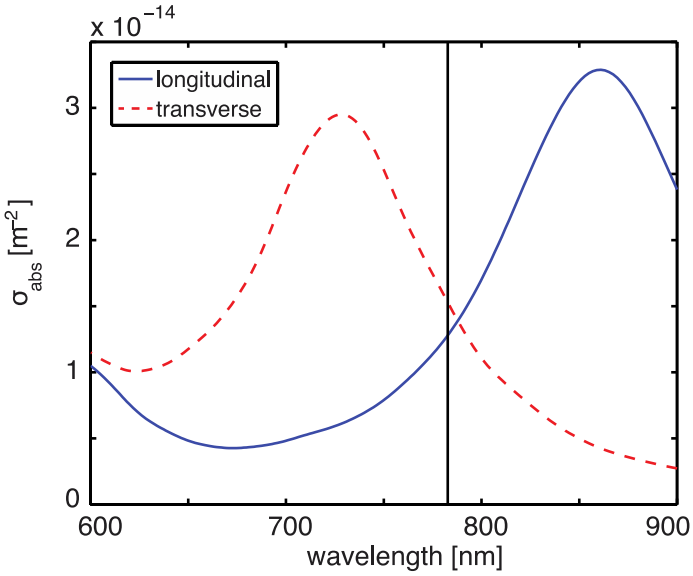

Figure S6. FDTD simulation of the absorption cross-section σ_{abs} as a function of wavelength for bowtie nanoantennas as described in the experimental section of the main text. The blue full line and the red dashed line show the results for longitudinal and transverse excitation. The excitation wavelength (785 nm) as used in our setup is indicated with a vertical black line.

Figures S5 and S6 show the simulated spectral response of the bowtie nanoantenna, respectively for the maximum field enhancement E_{max}/E_0 and the absorption cross-section σ_{abs} in both excitation modes. It is clear from both figures that the laser wavelength used in our experiments (785 nm, indicated with the solid black line) is not on the resonance of the nanostructures (which, however, is unimportant for all the effects reported in this paper).

5. Estimation of the optical field

We here present a calculation for the maximum optical electric field strength present in the plasmonic hotspot, based on results from our FDTD simulations (see Section 4 in this SI). For a focused laser beam of power P and diameter D, we approximate the intensity in the laser beam as $I_0 = \frac{4P}{\pi D^2}$. The intensity subsequently can be converted to an electric field strength E_0 by assuming $I_0 = \frac{1}{2} c n_e \epsilon_0 |E_0|^2$, where n_e is the refractive index of the medium, c is the speed of light in vacuum, and $\epsilon_0$is the electric permittivity of the vacuum. Using 1.33 as the refractive of the surrounding medium, we estimate the incident optical electric field strength at 5 mW to be 0.038 MV/cm. This leads to a maximum optical field strength in the gap of the bowtie antenna to be 1.5 MV/cm, using 40 as the electric field enhancement for longitudinal polarization. This is far below the threshold for pure optical breakdown[2], when no DC transmembrane bias would be applied.

6. Noise-spectra of plasmonic-breakdown-fabricated nanopore

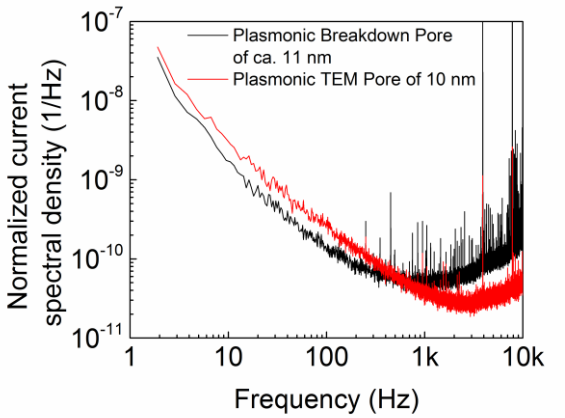

Figure S7. Normalized noise spectra (S_I/I^2) of a plasmonic nanopore made using plasmonic dielectric breakdown (black) and using TEM drilling (red). The figure shows that the low frequency noise of both nanopores is comparable.

7. Conductance versus diameter of plasmonic-breakdown-fabricated nanopores

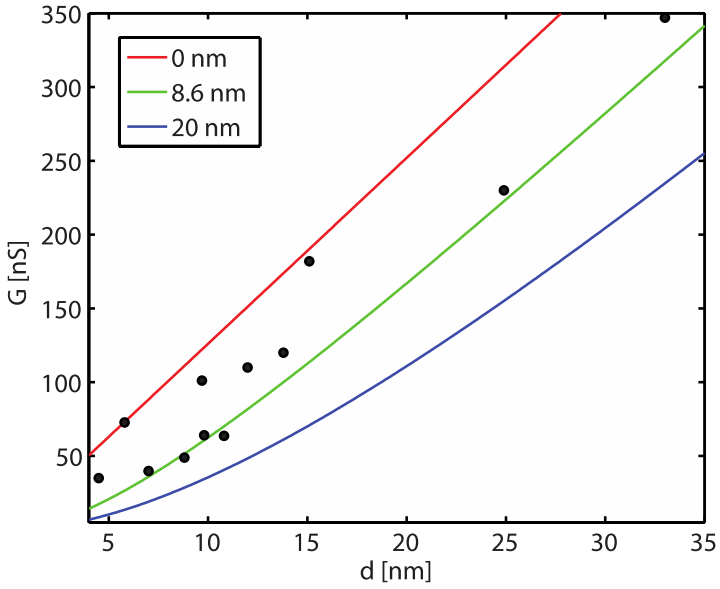

Figure S8. Conductance G of plasmonic breakdown nanopores versus diameter d as determined from TEM images (black circles). The equation of Kowalczyk *et al.* has been plotted for different values of the effective length l_{eff} = 0 nm (red, lower limit), 8.6 nm (green, estimated value for TEM-drilled pores) and 20 nm (blue, full membrane thickness, upper limit).

Figure S8 shows the measured nanopore conductance plotted versus the nanopore diameter, as determined from the TEM pore images. In the same plot, the hourglass model for nanopore conductance from Kowalczyk *et al.* is shown, using values for the effective pore length of 20 nm (perfect cylindrical pore), 8.6 nm (TEM hourglass-shaped pore) and 0 nm (extremely thin pore). The effective nanopore length corrects for the pore having an hourglass shape, i.e., not being a perfect cylinder that crosses the 20 nm thick membrane.

The measured values deviate from the model's prediction for a given value of effective pore length, where no single effective pore length fits the data well. The discrepancies might arise because of several reasons. First of all, the model used assumes a cylindrically symmetric

hourglass-shaped nanopore and a good fit of the model requires all pores to have a similar nanopore wall profile. However, the plasmonic breakdown method in general does not lead to cylindrically symmetric nanopores (as is already clear from the TEM images in Figure S1), nor will the wall profile of each pore be necessarily similar from pore to pore. Hence, expecting a good fit using from the model might be too optimistic. Second, the nanopore conductance was measured right after pore formation. Afterwards, pores were stored in an 1:1 ethanol:water mixture until TEM imaging up to 1 week later. In the mean time, pores could have grown in size, which could lead to larger pore sizes on the TEM images. Thus, the TEM-determined size will not accurately reflect the size at the time of the conductance measurement. Third, the nanopore diameter was determined from TEM imaging by approximating the area of the nanopore as a circle. The area often clearly did not resemble a circle, and hence this method might have led to additional errors.

8. Diameter and conductance determination of plasmonic nanopore used in DNA translocations

The estimated value for the diameter of the nanopore used for DNA translocations was 14.2 nm and 10.6 nm, as determined from the TEM image in Figure S1 (image indicated with a star) and the hourglass model for the nanopore conductance, respectively. To determine the diameter and effective length (4.3 nm) of the nanopore using the model, we used the measured pore conductance of 91 nS, the measured DNA conductance blockade of 3.2 nS conductance blockade (both measured at the start of the translocation experiment), and the 12.6 S/m conductivity of the 2 M LiCl (measured using Zetasizer Nano ZS (Malvern)). During the experiment, pore growth was observed for illumination powers above 2 mW, which resulted in an increased pore conductance of 120 nS and a DNA conductance blockade of 2.9 nS at the end of the translocation experiment. The latter values predict a pore diameter of 12.8 nm (and effective pore length of 2.9 nm), which is much closer to the 14.2 nm as measured from the TEM image.

9. Relative current increase versus laser power

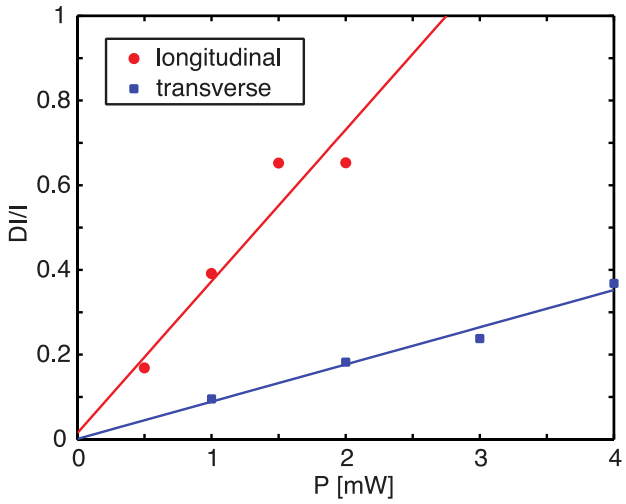

Figure S9. Relative current increase $\frac{DI}{I} = \frac{I_{laser} - I_{no\ laser}}{I_{no\ laser}}$ in longitudinal (blue) and transverse excitation (red) for nanopore used in DNA translocation experiment versus laser power *P* and linear fits.

The current through the nanopore can be used as an indication for the temperature near the nanopore. In the hourglass-shape geometrical model for the nanopore conductance, the only temperature dependent parameter is the buffer conductivity. Hence the relative conductance increase $\frac{DI}{I} = \frac{I_{laser} - I_{no\ laser}}{I_{no\ laser}}$ is solely determined by buffer conductivity.[3] Here I_{laser} is the current through the nanopore at a give laser power and $I_{no\ laser}$ is the current in absence of laser illumination. Hence, using Figure S9, we can deduce that laser illumination of this bowtie antenna in longitudinal mode leads to a temperature increase in 26 C/mW and 7.1 C/mW for the transverse mode.

References

(1) Keyser, U. F.; Krapf, D.; Koeleman, B. N.; Smeets, R. M. M.; Dekker, N. H.; Dekker, C. *Nano Letters* **2005**, *5* (11), 2253–2256.

(2) Lenzner, M.; Krüger, J.; Sartania, S.; Cheng, Z.; Spielmann, C.; Mourou, G.; Kautek, W.; Krausz, F. *Physical Review Letters* **1998**, *80* (18), 4076–4079.

(3) Jonsson, M. P.; Dekker, C. *Nano letters* **2013**, *13* (3), 1029–1033.